Comparing Concentrating-Solar-Power and Photovoltaic-Solar Plants as Extended-Duration Peaking Resources in Electricity Systems

Alexander Bard and Ramteen Sioshansi

Abstract This chapter compares the performance of two solar electricity-generation technologies with complementary energy-storage technologies—concentrating solar power (CSP) with thermal energy storage (TES) and photovoltaic (PV) solar with battery energy storage (BES)—in providing capacity during time periods with high electricity demand. We develop optimisation models, which determine the configuration and hourly operation of the two technologies, and apply the models to a case study that is based on the southwestern United States of America, which is a region that has excellent solar availability. Our models and case study demonstrate that PV with BES is superior to CSP with TES in terms of capital cost and peaking capability. Altogether, our results suggest that solar technologies can help to maintain reliable electricity supply under carbon constraints in regions of the world, such as east Asia, with relatively good solar resource. We conclude this chapter with a discussion of policy and regulatory changes that can help to achieve such an end.

Keywords Solar generation · Concentrating solar power · Thermal energy storage · Photovoltaic solar · Battery energy storage · Peaking generation · Capacity value

A. Bard
Department of Mechanical and Aerospace Engineering, The Ohio State University, Columbus, OH, USA
e-mail: bard.41@buckeyemail.osu.edu

R. Sioshansi (✉)
Department of Engineering and Public Policy, Carnegie Mellon University, Pittsburgh, PA, USA
e-mail: rsioshan@andrew.cmu.edu

Carnegie Mellon Electricity Industry Center, Carnegie Mellon University, Pittsburgh, PA, USA

Department of Electrical and Computer Engineering, Carnegie Mellon University, Pittsburgh, PA, USA

Wilton E. Scott Institute for Energy Innovation, Carnegie Mellon University, Pittsburgh, PA, USA

Department of Integrated Systems Engineering, The Ohio State University, Columbus, OH, USA

H. Phoumin et al. (eds.), *Tackling the Energy Transition: Insights from ASEAN and Beyond*, Climate Change and Energy Transition,
https://doi.org/10.1007/978-981-96-6019-3_6

1 Introduction

Solar generation can be enhanced significantly by integrating it with energy storage, which can help to manage variable solar availability, thereby making the generator partially dispatchable. Concentrating-solar-power (CSP) plants can benefit from thermal energy storage (TES), which is a relatively low-cost and efficient energy-storage technology that uses a constructed tank as the energy-storage medium (Peinado Gonzalo et al. 2019; Sun et al. 2021). Similarly, photovoltaic (PV) solar can be coupled with energy storage—for instance lithium-ion batteries, which is the technology that we consider in this study. Gami et al. (2017), Yagi et al. (2019), and Varghese and Sioshansi (2020) provide foundational studies of CSP, PV, and energy-storage technologies, and our current work builds upon these.

Integrating TES into CSP can enable the delivery of electricity during periods of low or zero solar availability (*e.g.*, during nights and cloudy time periods) or to desirable time periods (*e.g.*, of high energy prices or electricity demand). This benefit mirrors the capabilities of PV solar that is coupled with battery energy storage (BES). Historically, solar availability, wholesale energy prices, and electricity demand are fairly correlated in many electricity systems. These correlations are driven by air-conditioning demand during the summer, when solar availability tends to peak. The increasing penetration of solar energy is reducing these correlations (Ueckerdt et al. 2015). Thus, the ability of energy storage to align solar generation with peaks in energy prices and electricity demand will be of increasing value as the electricity-generation mix and demand patterns change.

This chapter investigates the potential of solar generation with energy storage to supply energy during peak-demand periods, considering future electricity systems that may have very different demand and supply patterns compared to today's systems. The ability of a resource to serve on-peak demand reliably often underlies a reliability or resource-adequacy assessment of an electricity system (Singh and Billinton 1977; Billinton and Allan 1984; Kim et al. 2022). A variety of metrics, including effective load-carrying capability (ELCC), can be used to determine the contribution of an individual resource to meeting an electricity system's reliability criteria (Garver 1966). These assessments involve applying reliability and statistical modeling to resource-availability and demand data. In some instances, approximations or heuristics are applied to avoid the computational cost of reliability modeling (Madaeni et al. 2013a).

Madaeni et al. (2012, 2013b) conduct ELCC analyses of CSP with and without TES. Their analyses make several assumptions, which we cannot apply, given our desire to understand solar technologies in future electricity systems. First, they analyze a well defined electricity system, with assumed known capacities and failure probabilities of each generator that is in the system. Second, they assume a known historical electricity-demand pattern. Their ELCC calculations are sensitive to the assumed demand pattern, due to the aforementioned historical correlation between solar availability and electricity demand. Consequently, their analysis is unlikely

to reflect accurately the contribution of solar generation to the reliability of future electricity systems (Yagi et al. 2019, 2021).

Unlike other electricity-generation technologies, solar resources exhibit declining marginal reliability benefit as their penetration levels increase (Awara et al. 2018). This decline arises from the real-time production of solar plants being highly correlated (energy production is driven by the same fundamental diurnal pattern). As such, each incremental solar generator that is added produces energy contemporaneously with the output of existing solar generators. This decline can be addressed through the use of energy storage, which is the focus of our analysis.

We overcome the complexities in assessing the reliability benefit to future electricity systems of solar generation, including its declining marginal benefit, by eschewing a formal reliability analysis. Rather, we use a less formal approach, whereby we examine whether the solar generator has sufficient energy available to operate at its nameplate capacity during a prescribed set of target hours of the modelled year (Yagi et al. 2019, 2021). By varying the target hours, we examine the performance of the solar generator *vis-à-vis* a varying reliability standard. Our primary performance metric of the solar generator is what we term its energy deficit, which is defined as the amount of additional energy that is needed for the generator to meet the prescribed performance target.

We evaluate and compare CSP with TES and PV solar with BES based on their energy deficits and estimated capital costs. Our findings suggest that attaining a given reliability level from CSP with TES is more expensive compared to doing so from PV solar with BES. This finding is reflective of significant recent decreases in the costs of PV-solar plants and BES systems. Although our analysis does not carry the rigor of a formal reliability analysis, it provides insights into the reliability benefits to future electricity systems of these technologies, a reliability analysis of which is exceedingly difficult to conduct.

The remainder of this chapter is organised as follows. Section 2 describes briefly the technologies that we study and their design and sizing characteristics. Section 3 details the models that are used in our analysis and defines formally the energy-deficit performance metric. Section 4 summarises our case-study data and results. Section 5 concludes, contextualises our results for decarbonising electricity systems globally and within east Asia, and discusses some policy, regulatory, and market-design considerations.

2 Technical Overview of CSP with TES and PV Solar with BES

Our analysis considers power-tower CSP plants. He et al. (2020) survey different CSP technologies, including power-tower, parabolic-trough, and linear-Fresnel systems. Power-tower CSP plants consist of three major components—a powerblock, a solar field, and a TES system. The powerblock converts thermal energy into electricity. Its

size is characterised normally by its nameplate input or output capacity, which are measured in MW-t and MW-e, respectively. The solar field is a collection of mirrors, known as heliostats. These are mounted onto double-axis solar-tracking systems and concentrate sunlight onto the plant's power tower, which collects the thermal energy. This thermal energy can be fed into the powerblock (to produce electricity) or into the TES system (to be stored for later use). The typical unit of measure for the solar field is its solar multiple, which gives the ratio between the nameplate thermal capacity of the powerblock and the thermal power that is collected by the solar field under reference conditions. The TES system can store thermal energy that is collected by the power tower but not used by the powerblock. The capacity of the TES system can be measured by its rated thermal-energy capacity (MWh-t). However, it is common to measure this capacity by the number of consecutive hours that the powerblock can operate at its nameplate capacity, solely using energy from a fully charged TES system. This latter measure is called the number of hours of storage.

These three components can be sized independently of one another. However, when considering plant configurations, it is common to hold the powerblock size fixed, because solar multiple and hours of storage are measured relative to this capacity. Moreover, it is common for each of solar-field and TES-system size to be chosen considering the size of the other component. For instance, increasing a plant's solar multiple allows the power tower to collect more thermal energy during periods with less-than-ideal weather conditions. However, the power tower collects excess thermal energy that must be rejected by the powerblock during peak-solar conditions. Increasing the size of the TES system allows this excess thermal energy to be stored for use during subsequent low-solar time periods. As such, optimising the design of a CSP plant requires considering weather conditions and solar-field and TES-system size holistically.

We model the PV solar and BES system as consisting of two key components—an array of PV panels and a set of batteries. The PV array is characterised by its nameplate capacity, measured either as MW-dc or MW-ac. The BES system is characterised by its power and energy capacities. The power capacity is the maximum charging and discharging rate of the BES system, measured in MW. The energy capacity can be measured in MWh. As with a TES system, it is common to measure the energy capacity of the BES system by the number of hours of storage, which gives the number of consecutive hours that the fully charged BES system can discharge at its power capacity.

3 Modelling Approach

This section provides detailed formulations of the models that we use to compare the cost and performance of the two solar electricity-generation technologies. The CSP-plant model assumes a fixed plant configuration and determines how to operate the plant to minimise its energy deficit. We use two model variants to study PV solar. Both variants of the model determine the sizes of the PV array and BES system

and how to operate the plant. The first variant minimises the plant's energy deficit subject to a constraint that limits the cost of the plant configuration. The second variant minimises the plant's cost with a constraint that limits the plant's energy deficit.

We take this modelling approach because it is reasonable to assume that the cost and performance of a PV array and BES system scale linearly with component sizes. Conversely, the performance and cost of a CSP plant's solar field scale non-linearly. This non-linearity stems from the field's physical properties, *i.e.*, its circular layout and the resultant changing marginal thermal-energy collection by each concentric ring of heliostats as the field size changes. As such, our modelling approach determines the cost and energy deficit of a given CSP-plant configuration and determines how the PV plant must be configured to achieve the same cost and energy deficit.

3.1 CSP-Plant Model

The CSP-plant model is patterned around the work of Sioshansi and Denholm (2010, 2013). The model takes as an input the hourly thermal energy that is collected by the plant's power tower, which depends upon a fixed plant configuration and assumed weather data. The model determines how to use the collected thermal energy—what amount is fed into the powerblock to produce electricity as opposed to being stored using the TES system. As needed, collected thermal energy can be supplemented with previously stored energy that is extracted from the TES system.

3.1.1 Model Notation

We begin by defining model notation. Because CSP plants convert thermal energy into electricity, we use the suffix '-t' to denote thermal power and energy. First, we define the following indices and parameters:

E_t^{R}	thermal power that is needed to start up the powerblock from an offline state (MW-t);
E_t^{W}	thermal power that is collected by the power tower during hour t (MW-t);
H	energy-storage capacity of the TES system (h);
K_t^{P}	hour-t energy-deficit penalty ($/MW);
l_0	ending hour-0 state of energy (SOE) of the TES system (MWh-t);
t	time index;
T	number of hours in optimisation horizon;
u_0	binary parameter that equals 1 if the powerblock is online during hour 0 and equals 0 otherwise;
$\theta^{\max}$	maximum input to the powerblock when it is online (MW-t);

$\theta^{\min}$ minimum input to the powerblock when it is online (MW-t); and

Υ self-discharge rate of the TES system (p.u.).

Next, we define the following decision variables:

l_t ending hour-t SOE of the TES system (MWh-t);

r_t binary variable that equals 1 if the powerblock is started up during hour t and equals 0 otherwise;

u_t binary variable that equals 1 if the powerblock is online during hour t and equals 0 otherwise; and

θ_t thermal power that is input to the powerblock during hour t (MW-t).

3.1.2 Model Formulation

The model is formulated as:

$$\min \sum_{t=1}^{T} K_t^{\mathrm{P}} \cdot (\theta^{\max} - \theta_t) \tag{1}$$

$$\text{s.t.} \theta^{\min} u_t \leq \theta_t \leq \theta^{\max} u_t - E_t^{\mathrm{R}} r_t, \forall t = 1, \ldots, T \tag{2}$$

$$r_t \geq u_t - u_{t-1}, \forall t = 1, \ldots, T \tag{3}$$

$$l_t \leq \Upsilon l_{t-1} + E_t^{\mathrm{W}} - E_t^{\mathrm{R}} r_t - \theta_t, \forall t = 1, \ldots, T \tag{4}$$

$$0 \leq l_t \leq H\theta^{\max}, \forall t = 1, \ldots, T \tag{5}$$

$$r_t, u_t \in \{0, 1\}, \forall t = 1, \ldots, T. \tag{6}$$

Objective function (1) minimises the plant's energy deficit over the T-hour optimisation horizon. For each $t = 1, \ldots, T$, the hour-t energy deficit is defined as the difference between the nameplate capacity of the powerblock, $\theta^{\max}$, and θ_t, which is the thermal power that is fed into the powerblock during hour t. Thus, the hour-t energy deficit measures the amount by which the plant operates below its nameplate capacity. The hourly energy deficits are multiplied by coefficients, $K_1^{\mathrm{P}}, \ldots, K_T^{\mathrm{P}}$, which reflect that depending upon how the performance requirement is set, plant operations may consider energy deficits only during a subset of what we term target hours that are within the optimization horizon. We set $K_t^{\mathrm{P}} = 1000$ for all $t = 1, \ldots, T$ that are target hours and $K_t^{\mathrm{P}} = 1$ for other hours. Setting K_t^{P} equal to a small strictly positive

value during non-target hours provides an incentive for the CSP plant not to curtail energy needlessly during these hours.

Constraint set (2) imposes bounds on the powerblock while it is online. Thermal power that is input to the powerblock is reduced during any $t = 1, \ldots, T$ when the powerblock is started up from an offline state, which is represented by having $r_t = 1$. On the other hand, if the powerblock is offline during a given $t = 1, \ldots, T$, this is denoted by $u_t = 0$. Constraint (2) for such $t = 1, \ldots, T$ forces $\theta_t = 0$. Constraint set (3) defines, $\forall t = 1, \ldots, T$, the value of r_t in terms of the values of u_{t-1} and u_t. Specifically, if $u_{t-1} = 0$ and $u_t = 1$, which means that the powerblock is offline during hour $(t-1)$ and online during hour t, r_t is forced to equal 1. Constraint set (4) imposes a standard energy-balance restriction to give the evolution of the SOE of the TES system from one hour to the next. Specifically, $\forall t = 1, \ldots, T$, the hour-t SOE is limited to be no greater than the sum of the previous hour's SOE (accounting for energy that is lost due to temperature loss of the storage medium) and power that is collected by the power tower during hour t, less the sum of power that is fed to the powerblock and to start up the powerblock during hour t. Constraints (4) are inequalities to allow excess thermal energy that cannot be stored to be curtailed. Constraint set (5) imposes SOE limits on the TES system and (6) imposes integrality restrictions on the two sets of binary variables.

3.2 PV Model

The PV model is built upon the work of Varghese and Sioshansi (2020). The model co-optimises the size of the PV array and BES system, as well as their operations. It takes as an input hourly weather-dependent factors, which specify the per-unit electricity output of the PV array.

3.2.1 Model Notation

Below, we define notation for the PV model, without repeating notation that is shared with the CSP-plant model. Because a PV plant does not convert thermal energy into electricity, all energy and power in the PV model are electric and no '-e' suffix is included in any definitions. Moreover, all energy and power quantities are assumed to be ac (as opposed to dc), using standard inverter performance characteristics in this conversion. The following parameters are model inputs:

$C^{\mathrm{B,E}}$ cost of BES-system energy capacity ($/MWh);
$C^{\mathrm{B,P}}$ cost of BES-system power capacity ($/MW);
$C^{\max}$ maximum allowable cost of the PV plant ($);
C^{PV} cost of PV capacity ($/MW);
E_t^{A} hour-t capacity factor of the PV array (p.u.);

$\Delta^{\max}$ maximum allowable energy deficit of the PV plant (MWh);
η round-trip efficiency of the BES system (p.u.);
λ_0 ending hour-0 SOE of the BES system (MWh); and
τ target PV-plant output (MW).

Next, we define the following decision variables:

B_t^{C} hour-t BES-system charging (MW);
B_t^{D} hour-t BES-system discharging (MW);
δ_t hour-t PV-plant energy deficit (MWh);
$\kappa^{\mathrm{B,E}}$ energy capacity of the BES system (MWh);
$\kappa^{\mathrm{B,P}}$ power capacity of the BES system (MW);
κ^{PV} capacity of the PV array (MW);
λ_t ending hour-t SOE of the BES (MWh); and
ξ_t hour-t PV-array electricity production that is supplied to the electricity system during hour t (MW).

3.2.2 Formulation of Energy-Deficit-Minimisation Model

The model is formulated as:

$$\min \sum_{t=1}^{T} K_t^{\mathrm{P}} \delta_t \tag{7}$$

$$\text{s.t.} \delta_t \geq \tau - \xi_t - B_t^{\mathrm{D}}, \forall t = 1, \ldots, T \tag{8}$$

$$0 \leq \xi_t + B_t^{\mathrm{C}} \leq E_t^{\mathrm{A}} \kappa^{\mathrm{PV}}, \forall t = 1, \ldots, T \tag{9}$$

$$\lambda_t = \lambda_{t-1} + \eta B_t^{\mathrm{C}} - B_t^{\mathrm{D}}, \forall t = 1, \ldots, T \tag{10}$$

$$0 \leq \lambda_t \leq \kappa^{\mathrm{B,E}}, \forall t = 1, \ldots, T \tag{11}$$

$$0 \leq B_t^{\mathrm{C}}, B_t^{\mathrm{D}} \leq \kappa^{\mathrm{B,P}}, \forall t = 1, \ldots, T \tag{12}$$

$$C^{\mathrm{B,E}} \kappa^{\mathrm{B,E}} + C^{\mathrm{B,P}} \kappa^{\mathrm{B,P}} + C^{\mathrm{PV}} \kappa^{\mathrm{PV}} \leq C^{\max} \tag{13}$$

$$\delta_t \geq 0, \forall t = 1, \ldots, T. \tag{14}$$

Objective function (7) minimises the plant's energy deficit and includes the coefficients, $K_1^{\mathrm{P}}, \ldots, K_T^{\mathrm{P}}$, to capture that the plant may seek to minimise its energy deficit during a subset of target hours during the optimisation horizon. For all $t = 1, \ldots, T$, (8) defines the hour-t energy deficit as the difference between the plant's target output level, τ, and its hour-t production, which is given by the sum of PV-array production, ξ_t, and BES output, B_t^{D}.

Constraint set (9) restricts the total energy that is used by the plant during each hour to be no greater than what the PV array provides. For each $t = 1, \ldots, T$, total energy that is used by the plant during hour t is defined as the sum of ξ_t and energy that is stored into the BES system, B_t^{C}. This sum is constrained to be no greater than the PV array's capacity, κ^{PV}, which is scaled by the array's hour-t capacity factor, E_t^{A}. Constraint set (9) does not allow the BES system to be charged using excess energy from the electricity system. Instead, we assume that the plant must rely upon excess energy from the PV array for any BES-system charging. We make this assumption because we do not want the PV plant to rely upon an external energy source to meet its reliability criterion. Constraint set (10) is the energy-balance constraint for the BES system and has an interpretation that is akin directly to (4). Constraint set (11) restricts the SOE of the BES system, based on the chosen capacity, and is akin directly to (5). Constraint set (12) restricts charging and discharging of the BES system based on its chosen power capacity. Budget constraint (13) ensures that the total cost of the PV array and BES system does not exceed the prescribed limit. Constraint set (14) ensures that the hourly energy deficits are non-negative.

3.2.3 Formulation of Cost-Minimisation Model

The model is formulated as:

$$\min C^{\mathrm{B,E}}\kappa^{\mathrm{B,E}} + C^{\mathrm{B,P}}\kappa^{\mathrm{B,P}} + C^{\mathrm{PV}}\kappa^{\mathrm{PV}} \tag{15}$$

$$\text{s.t.}\delta_t \geq \tau - \xi_t - B_t^{\mathrm{D}}, \forall t = 1, \ldots, T \tag{16}$$

$$0 \leq \xi_t + B_t^{\mathrm{C}} \leq E_t^{\mathrm{A}}\kappa^{\mathrm{PV}}, \forall t = 1, \ldots, T \tag{17}$$

$$\lambda_t = \lambda_{t-1} + \eta B_t^{\mathrm{C}} - B_t^{\mathrm{D}}, \forall t = 1, \ldots, T \tag{18}$$

$$0 \leq \lambda_t \leq \kappa^{\mathrm{B,E}}, \forall t = 1, \ldots, T \tag{19}$$

$$0 \leq B_t^{\mathrm{C}}, B_t^{\mathrm{D}} \leq \kappa^{\mathrm{B,P}}, \forall t = 1, \ldots, T \tag{20}$$

$$\sum_{t=1:K_t^{\mathrm{P}}>1}^{T} \delta_t \leq \Delta^{\max} \tag{21}$$

$$\delta_t \geq 0, \forall t = 1, \ldots, T. \tag{22}$$

Model (15)–(22) is identical to (7)–(14), with two differences. First, (15) minimises the cost of the combined PV array and BES system; (7) minimises its energy deficit. Second, (21) imposes an upper limit on the energy deficit of the PV array and BES system. Constraint (21) uses the aforementioned convention regarding the values of $K_1^{\mathrm{P}}, \ldots, K_T^{\mathrm{P}}$ by considering energy deficits only during hours $t = 1, \ldots, T$ with $K_t^{\mathrm{P}} > 1$. Models (7)–(14) and (15)–(22) can be thought of as having a dual relationship. Model (7)–(14) determines the minimal energy deficit that can be achieved with a given budget limit whereas (15)–(22) determines the cost-minimising design that achieves a given energy-deficit limit.

4 Case Study

4.1 Overview

We conduct a three-step analysis to compare the cost and technical characteristics of CSP and PV-solar plants. First, we solve (1)–(6) with a fixed configuration to determine the energy deficit of the CSP plant. Next, we use (7)–(14) to determine the minimal energy deficit that can be achieved by PV solar with BES that costs no more than the CSP plant that we model costs. Finally, we use (15)–(22) to determine the cost of designing a PV-solar plant with BES that has an energy deficit no greater than that of the CSP plant.

We examine first a base case, in which the eight highest-load hours of each day of the modelled year (using historical load data) are target hours. Then we conduct a parametric analysis in which we vary the number of target hours during each day between the one and the 24 highest-load hours of each day of the modeled year. The case in which the 24 highest-load hours of each day are target hours means that the objective is to have the plant operate at its target output continuously during every hour of the year.

All three of (1)–(6), (7)–(14), and (15)–(22) are formulated using version 3.6.10 of the AMPL mathematical-programming software package. The models are solved using version 22.1.1 of IBM ILOG CPLEX on a system with an eight-core Apple Silicon M2 processor and 8 GB of memory. Default AMPL and CPLEX settings are used.

4.2 Data

We assume a typical CSP-plant design with a powerblock with nameplate thermal-input and electric-output capacities of 538 MW-t and 222 MW-e, respectively, a solar multiple of 3.0, and 12 hours of TES. This plant configuration has a cost of $1.5 billion, based on data that are obtained from version 2021.12.02 of System Advisor Model (SAM) (Blair et al. 2014, 2018). Using SAM data, we estimate a PV-array cost of $960 000 per MW of rated dc capacity and energy- and power-capacity costs for BES of $282 790 MWh and $233 170 MW, respectively.

We model solar plants at a location near Boulder City, Nevada (at coordinates 35.80° N, 114.98° W), which has 7.60 kWh/m^2 of average daily direct normal irradiance (DNI). We use historical weather and load data for the year 2014. Specifically, we use modelled weather data, which are obtained from version 2.0.1 of National Solar Radiation Database (NSRDB) (Wilcox 2012; Sengupta et al. 2014a, b, 2018). The NSRDB data are processed using SAM to determine the hourly thermal energy that is collected by the CSP plant's power tower, *i.e.*, the values of $E_1^{\mathrm{W}}, \ldots, E_T^{\mathrm{W}}$. Similarly, SAM is used to determine from the NSRDB data the capacity factors of the PV array, *i.e.*, the values of $E_1^{\mathrm{A}}, \ldots, E_T^{\mathrm{A}}$.

Hourly year-2014 electricity-demand data for NV Energy, which is the utility that has Boulder City, Nevada within its geographical footprint, are obtained from Federal Energy Commission Form 714. Form-714 data are used to determine target hours.

When solving (1)–(6), we use the powerblock's nameplate thermal-input capacity, $\theta^{\max} = 538$, as the target operating level. After solving the model, the CSP plant's energy deficit is given by:

$$\sum_{t=1:K_t^P>1}^{T} (\theta^{\max} - \theta_t). \tag{23}$$

The energy deficit can be reported in absolute terms or as a percentage of the total energy that is needed to operate the CSP plant at its target level during all target hours. This total energy need is:

$$\sum_{t=1:K_t^{\mathrm{P}}>1}^{T} \theta^{\max}.$$

To model the PV plant, we set its target output level as $\tau = 222$, which is the nameplate electric-output capacity of the CSP plant. Constraint (13) requires a budget limit for the PV array and BES system, which we set as $C^{\max} = 1\,500\,000\,000$, which is the modeled CSP-plant cost. Constraint (21) requires setting an energy-deficit limit, $\Delta^{\max}$, for the PV plant. We set this as:

$$\Delta^{\max} = \sum_{t=1:K_t^{\mathrm{P}}>1}^{T} [\tau - F_t(\theta_t)]; \tag{24}$$

where $F_t(\cdot)$ is the hour-t heat-rate function of the CSP plant and is obtained from SAM. Equation (23) computes the energy deficit of the CSP plant in terms of additional thermal energy that is needed to operate the plant at is nameplate thermal-input capacity during all target hours. Equation (24) converts the thermal-energy deficit into an equivalent electrical-energy deficit. This is done by computing, $\forall t = 1, \ldots, T$ such that $K_t^{\mathrm{P}} > 1$, the difference between the CSP plant's nameplate electric-output capacity, which is $\tau = 222$, and its actual electric output, which is given by $F_t(\theta_t)$. The conversion of the CSP plant's energy deficit from thermal energy, as is given by (23), to electrical energy is necessary, because the PV plant does not use thermal energy as an input as a CSP plant does.

4.3 Results

4.3.1 Single-Day Results

Figure 1 illustrates the general framework for analysing our results. It shows the hourly operation of the modelled CSP plant during 1 August, 2014, which is a typical hot summer day with high solar availability. The bars that are labelled 'Solar-Field Energy' show hourly energy that is collected by the plant's solar field. The bars that are labelled 'TES SOE' show the beginning hourly SOE of the TES system. Thus, the sums of these two bars indicate the total energy that is available for use by the CSP plant during each hour. The bars that are labelled 'Powerblock Energy Input' indicate (the negative of) hourly energy (from the solar field or TES) that is input to the powerblock. These bars are negative to indicate that they represent a use of thermal energy. The blue horizontal line that is across a portion of the horizontal axis that is at the bottom of the figure indicates the eight highest-load hours of the day, which are the eight target hours. During this day (which is common of the summer) the eight highest-load hours are consecutive and occur during the afternoon (due to air-conditioning demand). It is common during the winter for there to be two load peaks, which correspond to morning and evening lighting and heating demands. The bars that are labelled 'Energy Deficit' (of which there are none, because the CSP plant experiences no energy deficits during the eight target hours of this day) indicate hourly energy deficits.

Figure 1 shows that the CSP plant operates at its nameplate capacity during 12 hours of the day that is shown, and meets its performance requirement during all eight target hours. This is typical of hot sunny days during the spring, summer, and autumn. The TES system does not reach its maximum energy-storage capacity. Indeed, the plant operates continuously beginning as of 25 July, 2014 until hour 20 of 1 August, 2014, due to an abundance of thermal energy that is gathered during these

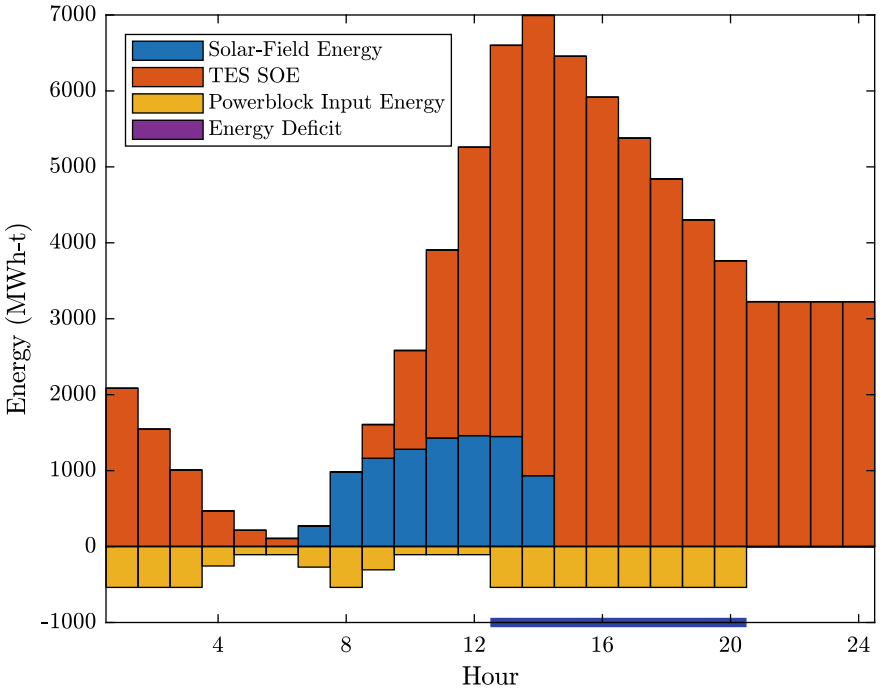

Fig. 1 Hourly thermal energy that is collected by the solar field, beginning TES-system SOE, powerblock input energy, and energy deficit for the modelled CSP plant during 1 August, 2014. The horizontal line that is across a portion of the horizontal axis indicates the eight highest-load target hours of the day

eight days. Excess thermal energy does not need to be stored for the plant to meet its performance requirement during the target hours of 1 August, 2014. Additionally, the CSP plant having sufficient energy to operate continuously during these eight days saves thermal energy that would be needed to start up a powerblock that is cycled to and from an offline state. Despite the abundance of solar energy, the TES system is valuable, in that it allows shifting solar energy to produce electricity during the load peak. Thermal energy that is collected by the solar field during 1 August, 2014 peaks between hours 9 and 13, but the load peaks between hours 13 and 20. The TES system allows the CSP plant to produce energy during the day's peak-demand hours.

Figure 2 summarises for the cost-minimising PV plant similar operational data to that which is presented for the CSP plant by Figure 1. Specifically, the bars that are labelled 'PV-Array Energy' and 'BES SOE' give the hourly amounts of electrical energy that is produced by the plant's PV array and the beginning hourly SOE of the plant's BES system. Thus, the sums of these bars indicate total electrical energy that is available to the plant during each hour. The bars that are labelled 'PV-Plant Output' indicate (the negative of) hourly electrical output of the PV plant to the electricity system. Electrical output can be from the PV array or by discharging the BES system.

The bars that are labeled 'Energy Deficit' and the blue horizontal line that is across a portion of the horizontal axis that is at the bottom of Figure 2 have the same interpretation as with Figure 1. Figure 2 shows that the PV plant performs similarly to the CSP plant *vis-à-vis* the target hours. A notable difference between the PV and CSP plants is that the former produces electricity during a longer window of time. This is due to a CSP plant being reliant upon DNI, which is reflected by the heliostats upon the power tower. A PV array is able to produce electricity using diffuse energy, which is available for more time (relative to DNI) during early mornings and late afternoons.

Figures 1 and 2 show that CSP and PV plants perform well with respect to providing energy during high-demand hours of sunny summer days. With low penetrations of wind and solar energy, these remain time periods with high electricity-supply needs. However, as the penetration of wind and solar increases, net electricity demands during sunny summer days will decrease, which will make other time periods more crucial. To understand the impacts of these changing load dynamics, Figures 3 and 4 provide the same operational results for the CSP and PV plants during 5 December, 2014 that Figures 1 and 2 do for 1 August, 2014. Unlike 1 August, 2014,

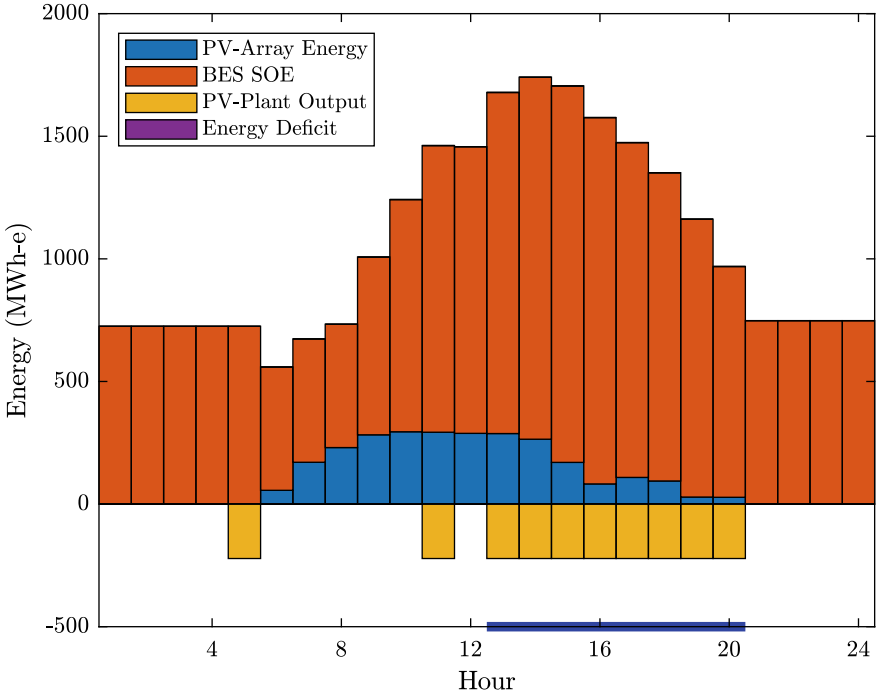

Fig. 2 Hourly electrical energy that is collected by the PV array, beginning BES-system SOE, PV-plant output, and energy deficit for the modelled cost-minimising PV plant during 1 August, 2014. The horizontal line that is across a portion of the horizontal axis indicates the eight highest-load target hours of the day

5 December, 2014 is a winter day with very limited solar availability. As such, both the CSP and PV plants experience energy deficits. Indeed, the CSP plant does not produce energy during any target hours between 2 December, 2014 and 4 December, 2014, due to the solar field not being able to collect any thermal energy during these days. As such, the CSP plant retains the stored energy in the TES system and uses it during 5 December, 2014 to meet the performance criterion partially. This is an optimal operational profile, because using the stored energy between 2 December, 2014 and 4 December, 2014 requires an additional powerblock start up, with associated energy losses. Because the PV plant uses diffuse solar radiation to produce electricity, it is able to meet partially the performance criteria between 2 December, 2014 and 4 December, 2014, due to some limited electricity output from the PV array during these days.

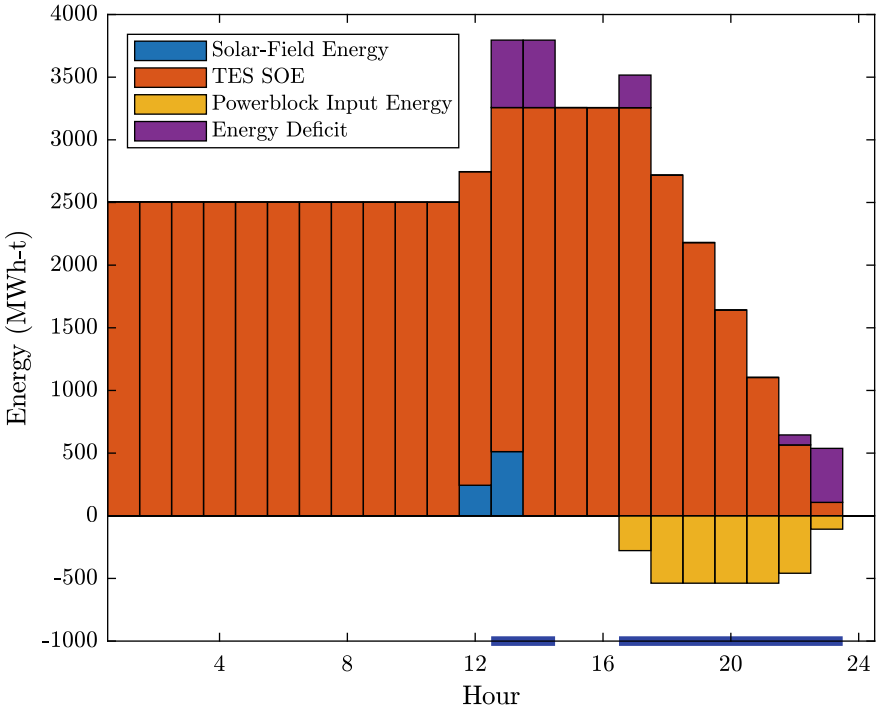

Fig. 3 Hourly thermal energy that is collected by the solar field, beginning TES-system SOE, powerblock input energy, and energy deficit for the modelled CSP plant during 5 December, 2014. The horizontal lines that are across portions of the horizontal axis indicate the eight highest-load target hours of the day

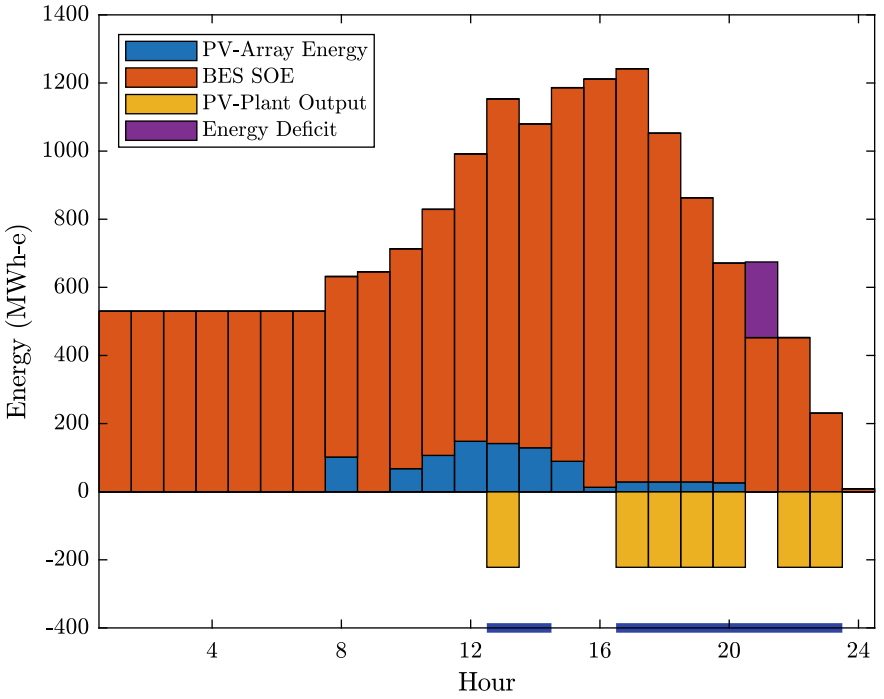

Fig. 4 Hourly electrical energy that is collected by the PV array, beginning BES-system SOE, PV-plant output, and energy deficit for the modelled cost-minimising PV plant during 5 December, 2014. The horizontal lines that are across portions of the horizontal axis indicate the eight highest-load target hours of the day

4.3.2 Optimal Plant Configurations, Costs, and Performance

Table 1 summarises the plant configurations. The CSP-plant configuration is fixed, as specified in Section 4.2. The two PV-plant configurations that are reported in Table 1 are optimised by solving (7)–(14) and (15)–(22), respectively. The table reports also each plant's total energy deficit during the year and its corresponding cost. Overall, the CSP plant is able to deliver 95.6% of the energy that is needed to meet the performance requirement, when it is applied to the eight highest-load hours of each day of the year. PV solar with BES can achieve the same overall performance, at a lower cost of $820 million, as opposed to $1.5 billion for the CSP plant. If a PV plant with BES can be built at the same $1.5 billion cost of the CSP plant, it delivers 99.66% of the energy that is needed to meet the performance requirement during the eight highest-load hours of each day of the year.

Although the PV plants have target electricity outputs of $\tau = 222$ MW-e, both the energy-deficit- and cost-minimising designs have oversized PV arrays with name-plate capacities of 703 MW-e and 338 MW-e, respectively. These design choices are akin to having a CSP plant with a solar multiple that is greater than 1.0. By oversizing

Table 1 Selected CSP-plant configuration, cost, and performance and optimised configuration, cost, and performance of PV plants

	CSP	Energy-Deficit-Minimising PV	Cost-Minimising PV
Nameplate Output Capacity (MW-e)	222	703	338
Hours of Energy Storage	12.0	10.2	6.3
Energy-Storage Power Capacity	538 MW-t	262 MW-e	222 MW-e
Energy Deficit (%)	4.4	0.34	4.4
Cost ($ million)	1 500	1 500	820

the PV array, the plant is able to produce 222 MW-e during a greater number of hours with less-than-ideal weather conditions. The cost-minimising PV-plant design has a BES system with a power capacity of 222 MW-e, meaning that the BES system is sized so that the PV plant operates at its target capacity entirely from stored energy. Conversely, the energy-deficit-minimising design has a BES system with a power capacity of 262 MW-e. This is because the BES is sized to charge a greater amount of excess PV output (from the significantly oversized PV array) to improve the plant's performance *vis-à-vis* the target hours.

Table 2 summarises the monthly energy deficits of the three plant configurations. The table provides insights regarding the relative performance of CSP and PV solar. Performance differences stem from fundamental differences between the physical properties of the two technologies. CSP requires high DNI and makes minimal use of diffuse solar radiation. This property of CSP is apparent in the energy deficits of the technologies during the cloudy (relative to other summer months) months of July and August. As a result, the CSP plant's energy deficit is one or two orders of magnitude greater than those of the two PV-plant configurations during these months. PV solar's improved performance is due to it being able to produce more energy during hours with low DNI (due to cloud cover) but with diffuse solar radiation being available. Conversely, the CSP plant outperforms the cost-minimising PV-plant design during the winter months of January and February, due to the CSP plant's larger energy-storage capacity. The energy-deficit-minimising PV plant is able to overcome this performance deficiency during the winter by increasing the size of the BES system from six to 10 hours of energy-storage capacity. Among the months of the year, December has a notably higher energy deficit that is one to six orders of magnitude larger compared to other months. This is expected, given weather patterns and limited daylight hours during December. Indeed, most of the energy deficit during December is accrued during the first two days of the month, which have particularly poor solar availability. Overall, the CSP plant has energy deficits during 128 hours of the year, as opposed to only 10 hours of energy deficits for the energy-deficit-minimising PV plant.

Table 2 Monthly energy deficits (%) of CSP and PV plants

	CSP	Energy-Deficit-Minimising PV	Cost-Minimising PV
January	0.068	0.009	0.096
February	0.045	0.001	0.060
March	0.013	0.000	0.004
April	0.001	0.000	0.001
May	0.000	0.000	0.001
June	0.000	0.000	0.001
July	0.013	0.000	0.001
August	0.026	0.000	0.001
September	0.009	0.000	0.001
October	0.007	0.000	0.009
November	0.016	0.001	0.036
December	0.320	0.032	0.317

4.3.3 Varying Target Hours

We conclude our case study by conducting a parametric analysis in which we vary the number of target hours during each day between the one and the 24 highest-load hours of the day. Table 3 summarises energy-deficit information for the CSP and energy-deficit-minimising PV plants with each number of target hours. Specifically, for each plant it reports the annual energy deficit as well as the deficit-weighted number of hours with energy deficits. The deficit-weighted number of hours with energy deficits for the CSP plant is computed as:

$$\sum_{t=1:K_t^{\mathrm{P}}>1,\theta_t<\theta^{\max}}^{T} \frac{\theta^{\max}-\theta_t}{\theta^{\max}};$$

whereas this value is computed as:

$$\sum_{t=1:K_t^{\mathrm{P}}>1,\delta_t>0}^{T} \frac{\delta_t}{\tau};$$

for the PV plant.

In most cases energy deficits are increasing in the number of target hours. However, CSP-plant performance improves slightly when the number of daily target hours increases from 15 to 16, from 17 to 18, and from 23 to 24. These improvements occur because increasing the number of target hours can change the target hours from occurring during two blocks of time during the day (*e.g.*, a morning and evening demand peak) to having a consecutive block of target hours. This change can be beneficial because of the energy that is consumed to shut down and start up the CSP

Table 3 Total energy deficits (%) and energy-deficit-weighted number of hours with energy deficits for CSP and energy-deficit-minimising PV plants with varying number of daily target hours

Number of Target Hours per day	CSP		Energy-Deficit-Minimising PV	
	Energy deficit	Deficit hours	Energy deficit	Deficit hours
1	0.00	0.00	0.27	0.97
2	0.03	0.22	0.14	0.99
3	0.53	5.82	0.09	0.99
4	1.30	18.97	0.07	0.99
5	2.00	36.43	0.05	0.99
6	2.84	62.29	0.10	2.25
7	4.12	105.35	0.27	6.79
8	4.39	128.21	0.34	9.90
9	6.48	212.75	0.55	18.18
10	7.60	277.22	0.86	31.21
11	8.61	345.66	1.06	42.68
12	9.94	435.51	1.36	59.36
13	11.10	526.75	1.79	84.96
14	12.56	641.96	2.21	112.97
15	13.93	762.76	2.63	144.11
16	12.85	750.65	3.07	179.19
17	16.83	1044.48	3.55	220.24
18	15.82	1039.45	4.12	270.53
19	20.46	1418.71	4.74	328.93
20	22.50	1642.50	5.62	410.35
21	24.64	1888.93	6.63	508.56
22	26.87	2157.70	8.16	651.71 lePara>
23	28.86	2423.14	9.59	805.11
24	27.23	2385.05	11.38	997.19

plant's powerblock if it must be cycled between two non-consecutive blocks of target hours. This phenomenon is notable when the number of daily target hours increases from 15 to 16, as the added target hour creates consecutive blocks of target hours during 21 days, which reduces by 12 the number of hours with energy deficits. If there are 24 daily target hours, then all 8,760 hours of the year are target hours and the CSP plant maximises energy production while it is online before exhausting stored energy and having to shut down the powerblock.

Figure 5 summarises the costs of the cost-minimising designs of PV plants with varying number of daily target hours. The costs of the PV-plant designs are not monotone in the number of daily target hours, which is to be expected, given the energy-deficit results that are reported in Table 3. For instance, increasing the number

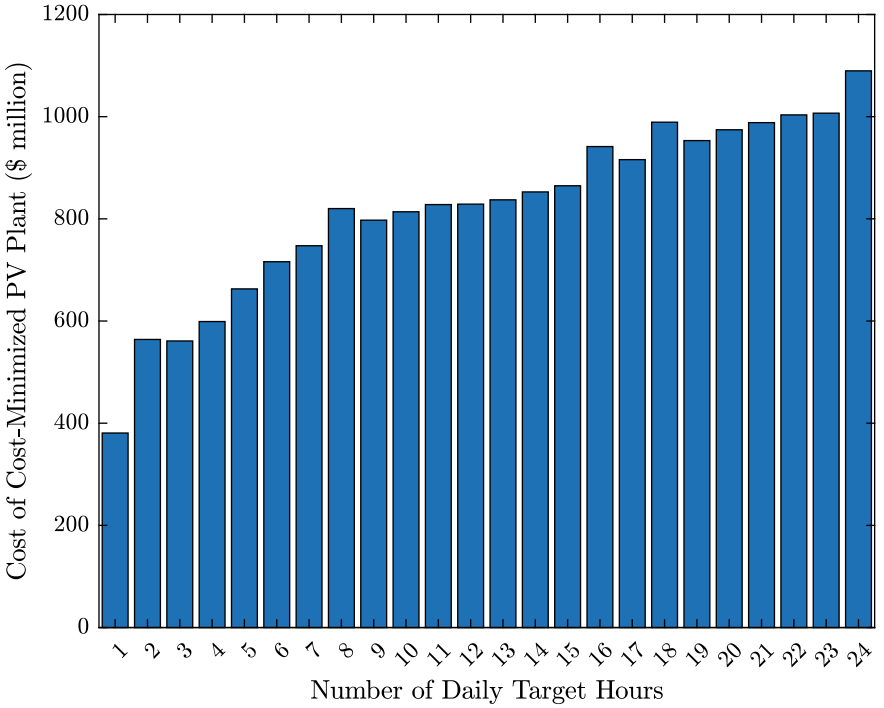

Fig. 5 Costs of cost-minimising PV plants with varying number of daily target hours

of daily target hours from 1 to 2 doubles the number of target hours. Yet, there is a negligible change in the energy deficit of the CSP plant. As such, the PV plant's design must be changed to meet the same performance criterion during twice as many hours. On the other hand, increasing the number of target hours from 18 to 19 yields a significant energy-deficit increase for the CSP plant. Because the PV plant is being designed to minimise cost while meeting the CSP plant's performance level, a less expensive plant design can be adopted with 19 target hours. Overall, Figure 5 shows that PV with BES can match the energy-deficit performance of CSP with TES at a much lower cost. This result is reflective of the significant decreases in the costs of PV modules and BES systems during the past several years (Fu et al. 2018; Cole et al. 2021).

5 Conclusions and Discussion

This chapter investigates the relative performance of two solar-electricity and energy-storage technologies—CSP with TES and PV solar with BES—as capacity resources. This focus is motivated by the fact that maintaining low-cost and reliable electricity

supply is a grand challenge of decarbonising electricity systems. Recent studies show that resource adequacy (*i.e.*, the ability to serve electricity demand reliably) will be a major challenge in planning and operating future electricity systems that cannot rely upon dispatchable fossil-fuelled generation (Cochran et al. 2021; Denholm et al. 2022). Moreover, these resource-adequacy challenges are known to become more acute during periods of limited wind and solar availability. This is because as wind and solar are added to an electricity system, peaks in the residual demand will be concentrated during periods of low wind and solar availability (*e.g.*, during the evening when electricity demand is high but solar availability is limited). Thus, the ability to serve these demands without using fossil fuels is critical. One may be tempted to dismiss these concerns as pertaining to future electricity systems. However, a series of rotating outages in California during 2020 is attributed to electricity-system planners not paying due attention to this phenomenon (CAISO, CPUC, and CEC 2021). In the same vein, these issues are important to efforts to decarbonise east-Asian electricity systems as that region of the world electrifies further.

We develop optimisation models to determine the operation and design of the CSP and PV plants and use energy deficit as our primary metric to measure the plants' abilities to serve electricity demand. Despite CSP being coupled with low-cost and efficient TES, we find that PV solar that is coupled with BES is a more cost-effective source of reliable electricity-system capacity. The poor cost performance of CSP is due, in part, to the cost of building its solar field, meaning that efforts to reduce these costs could improve CSP economics. PV solar benefits, also, from its modular design and deployment flexibility. CSP plants must be large to exploit economies of scale, whereas PV arrays can be deployed on greenfield or brownfield sites or on existing structures. Another possibility to improve CSP economics is to couple the technology with geological thermal energy storage (GeoTES) (Sharan et al. 2021; McTigue et al. 2023). As opposed to using constructed storage tanks (as is the case for TES), GeoTES uses existing abundant aquifers as the energy-storage medium. As such, the technology scales (*e.g.*, theoretically to thousands of hours of energy-storage capacity) much more cost-effectively compared to conventional TES. In addition, GeoTES has the potential to use geothermal energy to supplement solar-field energy. Calderón et al. (2018) survey other TES technologies that could improve CSP-plant economics further.

Decarbonising electricity systems while maintaining resource adequacy is not solely a technology challenge. Regulatory, policy, and market-design choices will impinge upon these outcomes (Conejo and Sioshansi 2019). Our work highlights the need for policies that incentivise the adoption of these technologies and address their integration into energy systems. Financial incentives, such as tax credits, subsidies, and feed-in tariffs, have proven effective in accelerating the deployment of renewable-energy technologies (Sioshansi 2016). These incentives should be structured to encourage innovation in energy-storage integration and efficiency improvements (Sioshansi 2011). The variable nature of solar availability necessitates policies that support electricity-system flexibility and stability (Mansouri and Sioshansi 2022). This includes investment in electricity-system infrastructure that is capable

of handling the variable output from solar plants and integrating them with existing and future energy sources (Yang et al. 2022).

Acknowledgements The authors thank A. Sorooshian and the editorial team for helpful discussions, comments, and suggestions. Any errors, opinions, and conclusions that are expressed in this paper are solely those of the authors.

Declarations

- Funding: This work was supported by The Ohio State University, National Science Foundation grants 1463492, 1808169, and 1922666, and Carnegie Mellon Electricity Industry Center.

References

Awara S, Zareipour H, Knight A (2018) Solar power capacity value evaluation—a review. In: 2018 IEEE Canadian Conference on Electrical & Computer Engineering, Institute of Electrical and Electronics Engineers, Quebec City, Quebec, Canada

Billinton R, Allan RN (1984) Reliability evaluation of power systems. Pitman Advanced Publishing Program, Boston, Massachusetts

Blair N, Dobos AP, Freeman J et al (2014) System Advisor Model, SAM 2014.1.14: General Description. Tech. Rep. NREL/TP-6A20-61019, National Renewable Energy Laboratory, Golden, CO

Blair N, DiOrio N, Freeman J et al (2018) System Advisor Model (SAM) General Description (Version 2017.9.5). Tech. Rep. NREL/TP-6A20-70414, National Renewable Energy Laboratory, Golden, CO

CAISO, CPUC, and CEC (2021) Root cause analysis: mid-August 2020 extreme heat wave. California Independent System Operator, California Public Utilities Commission, and California Energy Commission

Calderón A, Palacios A, Barreneche C et al (2018) High temperature systems using solid particles as TES and HTF material: a review. Appl Energy 213:100–111

Cochran J, Denholm P, Mooney M, et al (2021) The Los Angeles 100% Renewable Energy Study (LA100): executive summary. Tech. Rep. NREL/TP-6A20-79444-ES, National Renewable Energy Laboratory, Golden, CO

Cole W, Frazier AW, Augustine C (2021) Cost projections for utility-scale battery storage: 2021 update. Tech. Rep. NREL/TP-6A20-79236, National Renewable Energy Laboratory, Golden, CO

Conejo AJ, Sioshansi R (2019) Electricity market: a conversation on future designs. IEEE Power Energy Mag 17:18–19

Denholm P, Brown P, Cole W, et al (2022) Examining supply-side options to achieve 100% clean electricity by 2035. Tech. Rep. NREL/TP-6A40-81644, National Renewable Energy Laboratory, Golden, CO

Fu R, Feldman D, Margolis R (2018) U.S. solar photovoltaic system cost benchmark: Q1 2018. Tech. Rep. NREL/PR-6A20-72133, National Renewable Energy Laboratory, Golden, CO

Gami D, Sioshansi R, Denholm P (2017) Data challenges in estimating the capacity value of solar photovoltaics. IEEE J Photovoltaics 7:1065–1073

Garver LL (1966) Effective load carrying capability of generating units. IEEE Trans Power Apparatus Syst PAS-85:910–919

He YL, Qiu Y, Wang K et al (2020) Perspective of concentrating solar power. Energy 198:117373

Kim H, Sioshansi R, Lannoye E et al (2022) A stochastic-dynamic-optimization approach to estimating the capacity value of energy storage. IEEE Trans Power Syst 37:1809–1819

Madaeni SH, Sioshansi R, Denholm P (2012) Estimating the capacity value of concentrating solar power plants: a case study of the Southwestern United States. IEEE Trans Power Syst 27:1116–1124

Madaeni SH, Sioshansi R, Denholm P (2013a) Comparing capacity value estimation techniques for photovoltaic solar power. IEEE J Photovoltaics 3:407–415

Madaeni SH, Sioshansi R, Denholm P (2013b) Estimating the capacity value of concentrating solar power plants with thermal energy storage: a case study of the Southwestern United States. IEEE Trans Power Syst 28:1205–1215

Mansouri MA, Sioshansi R (2022) Using interim recommitment to reduce the operational-cost impact of wind uncertainty. J Mod Power Syst Clean Energy 10:839–849

McTigue JD, Zhu G, Akindipe D, et al (2023) Geological thermal energy storage using solar thermal and Carnot batteries: techno-economic analysis. Tech. Rep. NREL/CP-5700-87000, National Renewable Energy Laboratory, Golden, CO

Peinado Gonzalo A, Pliego Marugán A, García Márquez FP (2019) A review of the application performances of concentrated solar power systems. Appl Energy 255:113893

Sengupta M, Habte A, Gotseff P et al (2014a) A physics-based GOES product for use in NREL's National Solar Radiation Database. Tech. Rep. NREL/CP-5D00-62776, National Renewable Energy Laboratory, Golden, CO

Sengupta M, Habte A, Gotseff P et al (2014b) A physics-based GOES satellite product for use in NREL's National Solar Radiation Database. Tech. Rep. NREL/CP-5D00-62237, National Renewable Energy Laboratory, Golden, CO

Sengupta M, Xie Y, Lopez A et al (2018) The National Solar Radiation Data Base (NSRDB). Renew Sustain Energy Rev 89:51–60

Sharan P, Kitz K, Wendt D et al (2021) Using concentrating solar power to create a geological thermal energy reservoir for seasonal storage and flexible power plant operation. J Energy Resour Technol 143:010902

Singh C, Billinton R (1977) System reliability modelling and evaluation. Hutchinson Educational Publishers, London, UK

Sioshansi R (2011) Emissions impacts of wind and energy storage in a market environment. Environm Sci Technol 45:10728–10735

Sioshansi R (2016) Retail electricity tariff and mechanism design to incentivize distributed renewable generation. Energy Policy 95:498–508

Sioshansi R, Denholm P (2010) The value of concentrating solar power and thermal energy storage. IEEE Trans Sustain Energy 1:173–183

Sioshansi R, Denholm P (2013) Benefits of colocating concentrating solar power and wind. IEEE Trans Sustain Energy 4:877–885

Sun Z, Su L, Gao X et al (2021) Influences of impurity Cl^- on the thermal performance of solar salt for thermal energy storage. Solar Energy 216:90–95

Ueckerdt F, Brecha R, Luderer G (2015) Analyzing major challenges of wind and solar variability in power systems. Renew Energy 81:1–10

Varghese S, Sioshansi R (2020) The price is right? How pricing and incentive mechanisms in California incentivize building distributed hybrid solar and energy-storage systems. Energy Policy 138:111242

Wilcox SM (2012) National solar radiation database 1991–2010 update: user's manual. Tech. Rep. NREL/TP-5500-54824, National Renewable Energy Laboratory, Golden, CO

Yagi K, Sioshansi R, Denholm P (2019) Evaluating a concentrating solar power plant as an extended-duration peaking resource solar energy. Solar Energy 191:686–696
Yagi K, Sioshansi R, Denholm P (2021) Using concentrating-solar-power plants as economic carbon-free capacity resources. Energy Convers Manag: X 12:100112
Yang J, Dong ZY, Wen F et al (2022) Enhancing hosting capability for renewable energy generation in active distribution networks. IET Renew Power Gener 16:651–654